ISSN 1112-9867

Available online at

http://www.jfas.info

# NUMERICAL STUDY OF THIN FILM OXIDE EFFECT WITH MULTIPHYSICS COUPLING ON ELECTRICAL CONTACT PARAMETERS UNDER LOW FORCE

Hans Essone Obame\*, Honoré Gnanga, Arsène Eya'a Mvongbote

Laboratoire Pluridisciplinaire de Sciences (LAPLUS), Ecole Normale Supérieure, BP :17009, Libreville, Gabon

Received: 06 December 2023 / Accepted: 27 December 2023 / Published: 28 December 2023

#### **ABSTRACT**

Electrical contacts consist of parts where the surfaces in contact can carry electrical current just in a few contact asperity points scattered over the entire apparent contact area. Contamination and oxidation are inevitable on contact surfaces, especially for small contact under low force (mN). This oxidation phenomenon is accelerating by harsh environments (high temperature and high relative humidity RH), making then a thin film oxide on the interface. According to oxide thickness, the electrical resistance will varies allowing then a contact dysfunction. A finite element model has been used to study the multiphysics of thermo electromechanical phenomena and to analyze different cases and various physical parameters. The influence of contact structure on contact resistance was analyzed and the constriction resistance was extracted from measured resistance using a sample numerical simulation.

**Keywords:** Electrical contact, thin film oxide, finite elements model, multiphysics coupling

Author Correspondence, e-mail: hans.essone@mail.com

rumor correspondence, e man. nans.essonetaman.com

doi: http://dx.doi.org/10.4314/jfas.1357

## 1. INTRODUCTION

Often overlooked, electrical contacts play a crucial role in a wide range of applications such as automotive, aerospace, industry, and even residential settings. The insulating films that develop on contact surfaces are identified as a primary cause of contact failures. These unavoidable insulating films, resulting from processes like oxidation, contamination, or corrosion, form on contact interfaces and can impede current flow, leading to increased resistance [1, 2]. Unlike conventional contacts where applied forces [3] and currents can break down potential contamination, this becomes challenging at smaller scales (µm-mm). Typically, contact surfaces are naturally covered with metal oxides [4]. The composition and thickness of these oxide films vary depending on the type of metal, with common materials like aluminium, copper, or tin being susceptible to oxidation and corrosion. This paper also aims to explore how the corrosion of a copper alloy contact in a harsh environment with elevated temperature and relative humidity (RH) indirectly affects electrical contact resistance. These environmental factors are known to contribute to the degradation of copper, aluminium, and certain alloys commonly used in the electronic industry, particularly in developing countries. The study focuses on understanding how harsh environmental conditions impact stationary electrical contacts during aging, characterized by elevated environmental parameters. A comprehensive numerical investigation into film thickness, electrode size, substrate thickness, and the properties of both the film and substrate is crucial for advancing thin film science, nano-electronics, and biomedical diagnostic applications. The analysis of constriction resistance will specifically examine a two-dimensional asymmetric elastic-plastic spherical contact, considering a thermoelectromechanical model.

## 2. GENERAL CONSIDERATIONS AND MODEL EQUATIONS

Figure 1 illustrates an electrical contact between two conductors. In this scenario, the regime is locally ohmic, signifying that the local form of Ohm's law is applicable throughout:

$$\vec{E} = -\overline{grad} \, V = \rho \, \vec{J} \tag{1}$$

 $\vec{E}$ : Electric field vector

V: Electric potential

J: Current density vector

Ohmic resistance Re of the two conductors is calculated by the following relation:

$$R_e = \rho \frac{l}{A} \tag{2}$$

Where *l* is length and *A* section area.

The mechanical load F is carried by the asperities in contact. The size of the mechanical contact A can be described by the relationship between the hardness H and the load as equation (3) shows.

$$A = \frac{F}{H} \tag{3}$$

The electrical contact area is consequently smaller than the physical contact area, as illustrated in the three types of contact areas below: the apparent area, also referred to as the nominal contact area; the bearing area, which supports the mechanical load; and the area through which electrical current exclusively passes—the electrical contact area.

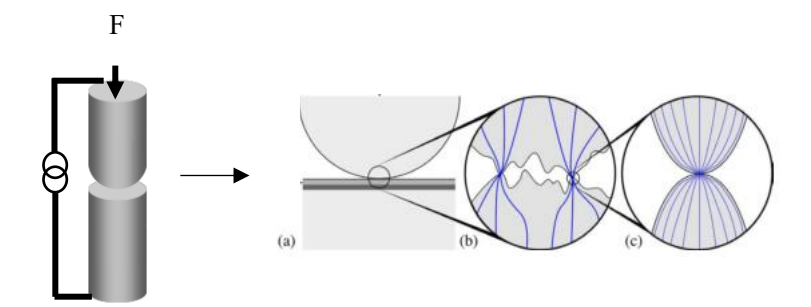


**Fig.1**. Separation of scales in the electric and mechanical contact between rough solids: (a) the macroscopic scale is characterized by nominally flat (smooth) surfaces, (b) at certain magnification the discrete nature of the contact is revealed. The real contact area is considerably smaller than the nominal contact area predicted at macroscopic scale with the Hertz contact theory; the real contact area can be approximated by a set of a-spots (c)

Nevertheless, the effective size (a) of the contact spot, commonly known as the a-spot responsible for current transfer, is merely a fraction of the mechanically loaded area. This size is predominantly influenced by the presence of the oxide layer and other impurities that coat the metallic contact surface. Holm [5] demonstrated that the constriction resistance (Rc), assuming equal metal resistivity ( $\rho$ ) on both components, can be computed as:

$$R_c = \frac{\rho}{2a} \tag{4}$$

Where a is the average radius of a-spots.

In the scenario where a poorly conductive oxide film separates the two elements at the contact point, the electrical properties of the film are typically intricate and, of course, contingent on the nature of the elements present on the contact surfaces within the interface and environment. It is worthwhile to consider these properties by defining a surface resistivity ( $\lambda$ ) in ohm-meters squared ( $\Omega$ .m<sup>2</sup>). In this case, the contact resistance is the aggregate of the constriction resistance and the film resistance, expressed as [6, 7]:

$$R_c = \frac{\rho}{2a} + \frac{\lambda}{\pi a^2} \tag{5}$$

In situations where a layer with thickness e and resistivity  $\rho c$  is positioned between the contact elements, both composed of the same resistivity material  $\rho$ , the contact resistance is formulated as [6, 7]:

$$R_c = \frac{\rho}{2a} + \rho_c \frac{e}{\pi a^2},$$
 (6)  
with  $\rho_c e = \lambda$ 

This formula remains applicable even in the absence of an intermediate layer; it is simply necessary to set e=0. The expression is grounded on the assumption that the resistance attributed to the presence of a layer arises solely from the conduction through this layer of resistivity  $\rho c$ . The formation of the oxide film results from surface contamination by atoms or molecules present in the atmosphere. The presence of an oxide film is particularly detrimental to electrical contacts because metal oxides exhibit high insulating properties. Just a few atomic layers are adequate to disrupt the electrical contact.

Figure 2 presents a schematic representation of constriction through a contact asperity involving the material and oxide layer. These coatings may consist of various layers designed to establish optimal bonding to the substrate, gradually transitioning towards the contact surface to achieve optimal contact properties.

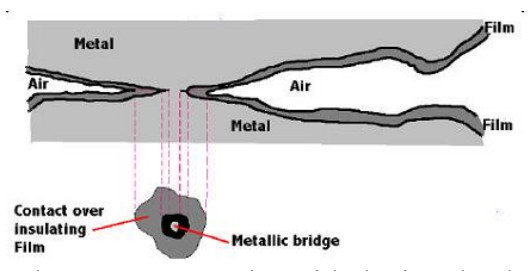


**Fig.2.** Constriction through a contact asperity with the involved material and oxide layer Copper undergoes oxidation in the presence of moist air, a process that accelerates notably with

increasing temperature. The rate of oxidation is influenced by the surface condition, level of hardening, and purity of the copper. The resulting oxide layer is highly electrically insulating, necessitating the application of a protective layer for use in electrical contacts.

The composition of the oxide film is contingent on operating conditions such as temperature, oxygen pressure, and the duration of the reaction. At temperatures below 150 °C, only cuprous oxide (Cu<sub>2</sub>O) with a red ruby color is formed [7-9]. Beyond 150 °C, the oxidation film consists of copper Cu<sub>2</sub>O oxides, incorporating CuO oxide with a green hue, as described by the reaction:

$$2CuO \to Cu_2O + \frac{1}{2}O_2 \tag{7}$$

The proportion of CuO in the oxidation of copper increases with temperature and is influenced by the duration of the oxidation process. However, at very high temperatures, it tends to decrease and eventually reaches a constant value. Various publications confirm the formation of Cu<sub>2</sub>O on copper at room temperature. The presence of moisture or gases, such as SO<sub>2</sub> and CO<sub>2</sub>, significantly affects the modification of the oxidation rate. Table 1 presents some results from the literature regarding the oxidation of copper under atmospheric pressure at different temperatures:

Table 1. Copper oxides thicknesses for different temperatures

Temperature (K)	Time (hours)	Oxide thickness (Å)
293	4	15
393	20	17
423	20	437

Accurately observing and experimentally characterizing the properties of these films, which are not well understood, can be challenging. Modeling and numerical simulation serve as suitable alternative approaches.

A numerical simulation, grounded in the Holm theory, stands out as one of the most robust tools for estimating constriction resistance [10-12]. This model concurrently addresses structural, thermal, and current flow considerations. The dependent variables in the model are the electric potential (V), temperature (T), and the displacement field (u). The simulation focuses on steady-state conditions, resembling those found in a stationary direct current contact. The software employed for this purpose is COMSOL Multiphysics [13].

#### 2.1. Mechanical model

The mechanical structural module [10] is integrated into the comprehensive model as a stationary elasto-plastic problem, responding to the applied force through contacts. The load between two spherical surface asperities can be assessed using a Hertzian pressure distribution, as described by equation [10].

$$p(r) = p_{max} \sqrt{1 - \frac{r^2}{R_c^2}} \tag{8}$$

The bottom boundary, as well as the right vertical boundary, is subject to roller constraints. This implies that motion in the direction normal to the surface is restricted, while it is free to move in the tangential direction of the surface.

#### 2.2. DC electrical model

In a conductive medium, the electrical charge conservation is given by:

$$\vec{\nabla}.\vec{J} = -\partial q_{el}/\partial t \tag{9}$$

where J is the density of the electric field (A/m) qel is the density of the electrical charge. We assume the potential field is quasi-static which reduces the Eq. (9) to the following:

$$\vec{\nabla}.\vec{J} = 0 \tag{10}$$

The Ohm's law allows us to express the current density as

$$\vec{J} = \sigma_{el}\vec{E} + \vec{J}_{el} \tag{11}$$

where  $\sigma$ el is the electrical conductivity [S/m];  $\vec{E}$  is the electrical field [V/m] and  $\vec{J}_{el}$  is the density of the external current generated [A/m], which is supposed nil in this study. Joule's law allows us to express the volumetric heat source (Joule heating) per time unit as

$$Q = J E \tag{12}$$

The electrical field may, also, expressed as a gradient of the electrical potential V as

$$\vec{E} = -\vec{\nabla}V \tag{13}$$

Therefore, equation (13) becomes:

$$\vec{\nabla}.\vec{E} = \vec{\nabla}.(\sigma_{el}\vec{E}) = \vec{\nabla}.(-\sigma_{el}\vec{\nabla}V) \tag{14}$$

The top surface is grounded over the distance a on the a-spot, and on the bottom surface, a normal current density is applied as the electrical load in the model.

#### 2.3. Heat transfer boundary condition

The outer side boundaries are configured similarly to the electrical case, meaning they are thermally insulated. The heat flux over the surface is zero, as indicated by the equation:

$$\vec{n}.(k\vec{\nabla}T) = 0 \tag{15}$$

 $\vec{n}$  is the normal vector of the boundary surface, k is the conductivity and T is the temperature. The temperature on bottom boundary is set to 293K.

Prior finite element simulation models have demonstrated the heat generation within the coating substrate in two-dimensional models [14-16] when a current passes through a contact a-spot. Further exploration, incorporating the mechanical load in the model and solving for the combined electromechanical model [14-16], reveals the impact on stresses within the coating substrate of the system. This paper expands on these findings by incorporating the three-dimensional effects of a tractive force on the material's stresses.

**Table 2.** Properties of material data used in the model collected.

Duon oution	Cu-Be	Cu2O	CuO
Properties	(Substrate)	(Coating1)	(Coating2)
Young's modulus [GPa]	130	82	100
Poisson's ratio	0.3	0.33	0.34
Density [kg/m3]	8260	6000	6990
Coefficient of thermal expansion 10 <sup>-6</sup> [1/K]	17.8	3	4
Thermal conductivity [W/mK]	130	4.5	98
Heat capacity at constant pressure [J/kgK]	418.6	60	52.6
Electric conductivity 106 [S/m]	12.6	50	2

The geometry is constructed based on the specified parameters within a single part. This part is segmented into an a-spot part, with a size denoted as 'a,' where current and heat transfer occur, and a load-carrying part, with a size denoted as 'Rc,' where the load is defined. The thickness of the coating material is determined by the coating thickness, denoted as 'ct.' Figure 3 illustrates the geometry with the utilized geometric parameters.

The a-spot and resistive film regions around the contact were modeled using a fine mesh, while the rest of the block and the sphere were meshed using a coarser mesh. This meshing technique enables the use of a finer mesh in the critical region, enhancing accuracy while maintaining a relatively low overall number of elements.

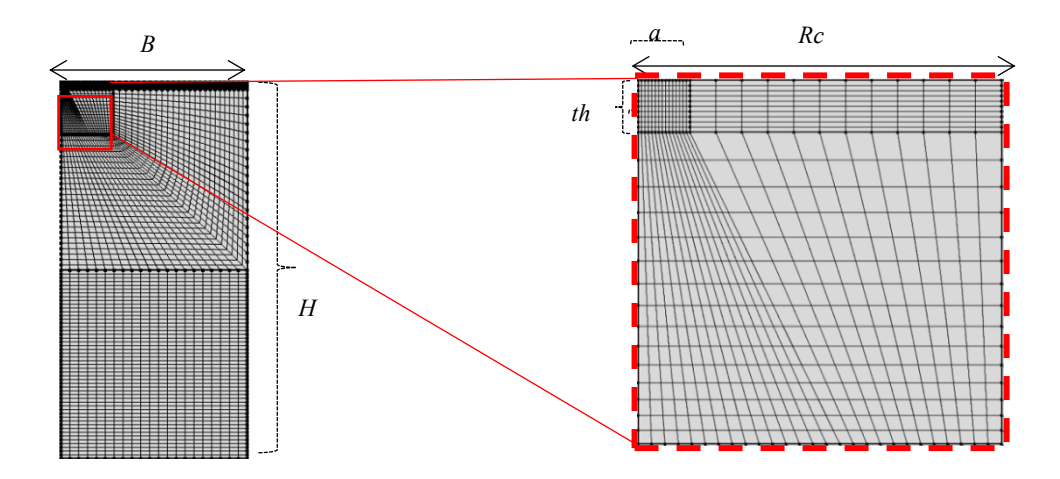


Fig.3. Geometry of the axisymmetric finite element model

#### 3. RESULTS AND DISCUSSION

Numerical simulations were conducted for various cases to explore the impact of resistive film and elastic deformation on electrical contact resistance and the radius of contact. Figure 4 illustrates the distribution of Von-Mises stress under load from a spherical indent with no current. Across the three materials, there is no alteration in mechanical stresses.

In Figure 5, the voltage drop across the sphere and the block is depicted. It is evident that the majority of the voltage drop occurs in proximity to the contact.

The temperature profile, as shown in Figure 6, indicates that the high temperature during the contact is highly localized, attributed to the bottleneck effect of the contact region.

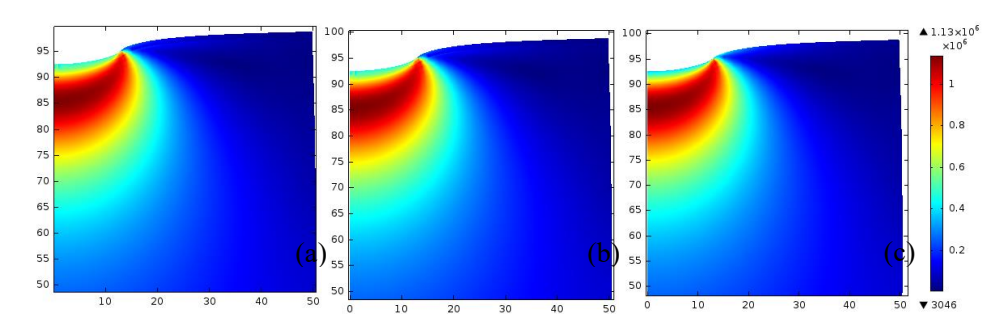


**Fig.4.** Distribution of Von-Mises stress near the contact area Model under pressure load and I=1A. Maximum shear stress [MPa]. (a)CuO/(b)Cu<sub>2</sub>O/(c)Cu-Be

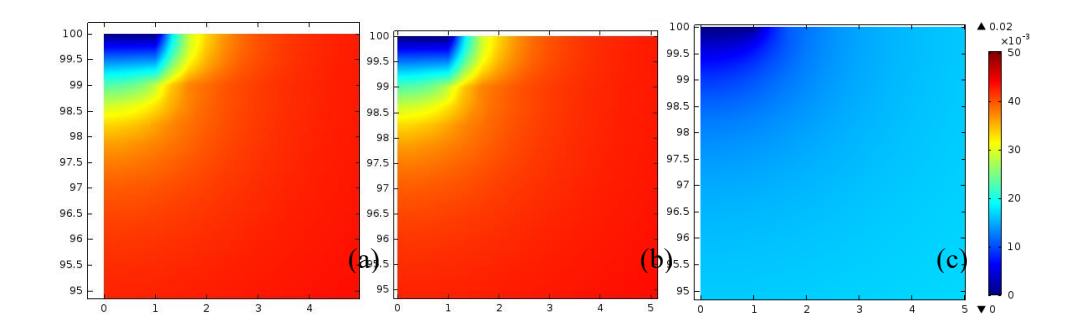
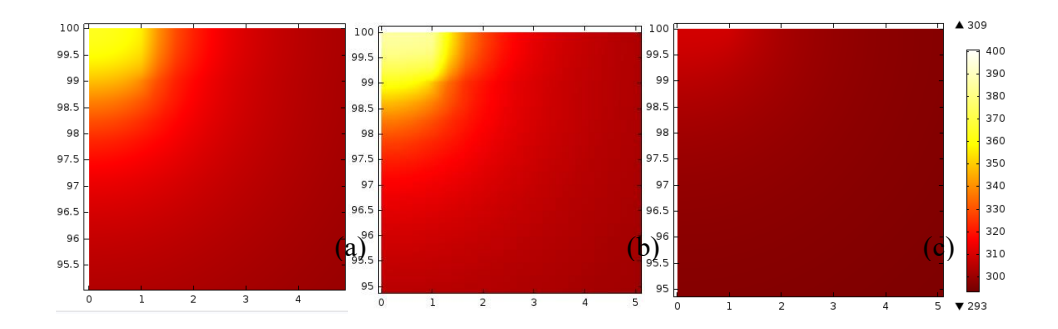


Fig.5. Voltage drop across the contact region (in V).(a) CuO/(b)Cu2O/(c)Cu-Be



**Fig.6.** Temperature profile in the spherical asperity and the block in degrees.

(a)CuO/(b)Cu<sub>2</sub>O/(c)Cu-Be

Electrical contact resistance values are determined by dividing the potential difference across the contact zone by the total current passing through the contact.

In the presence of Cu<sub>2</sub>O on the contact surface, an interesting relationship between contact voltage and current is observed, as depicted in Figure 7. The contact voltage increases with current, and this effect is more pronounced for smaller contact areas. This behavior is attributed to the varying electron transport properties of Cu<sub>2</sub>O under different current densities. Additionally, constriction resistance is inversely proportional to the contact area, implying that smaller contact areas exhibit higher resistance, as shown in Figure 8.

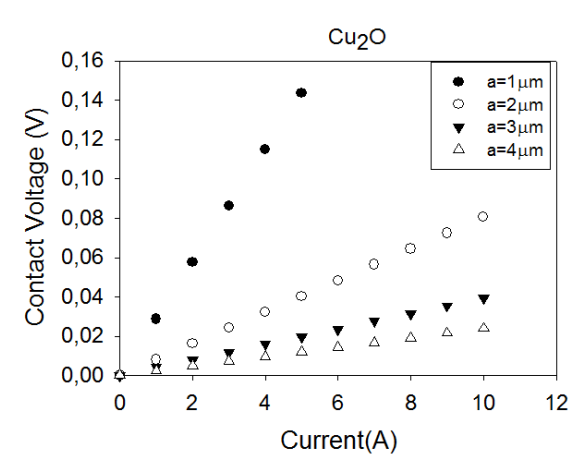


Fig.7. Contact voltage vs current for different a-spot radius. (Cu<sub>2</sub>O)

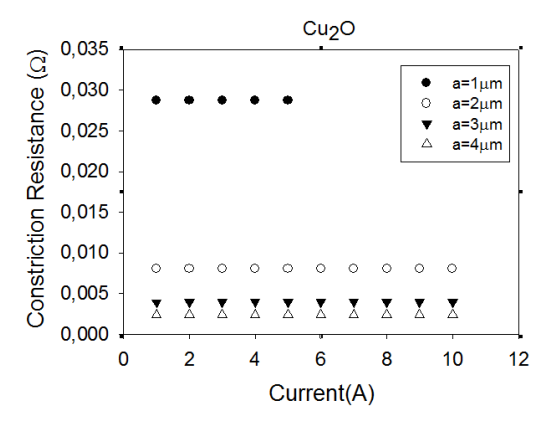


Fig.8. Constriction resistance vs current for different a-spot radius. (Cu<sub>2</sub>O)

A parallel trend is observed for temperature, as illustrated in Figure 9. Smaller contact areas lead to elevated temperatures due to increased current density. Interestingly, the effect of oxide thickness becomes particularly significant for smaller contact areas, emphasizing that oxide thickness plays a critical role in determining contact behavior in these cases.

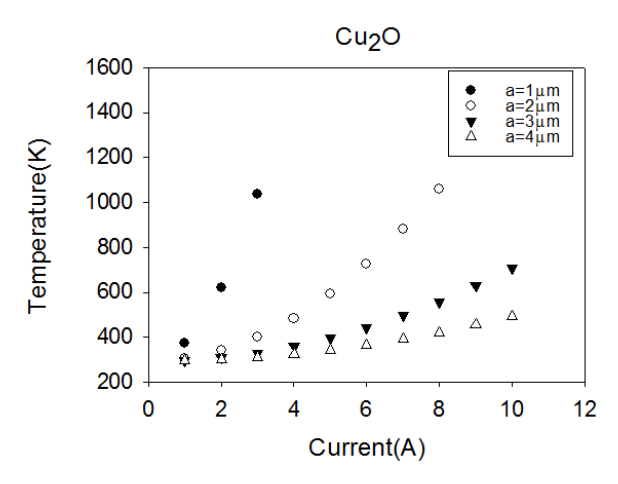
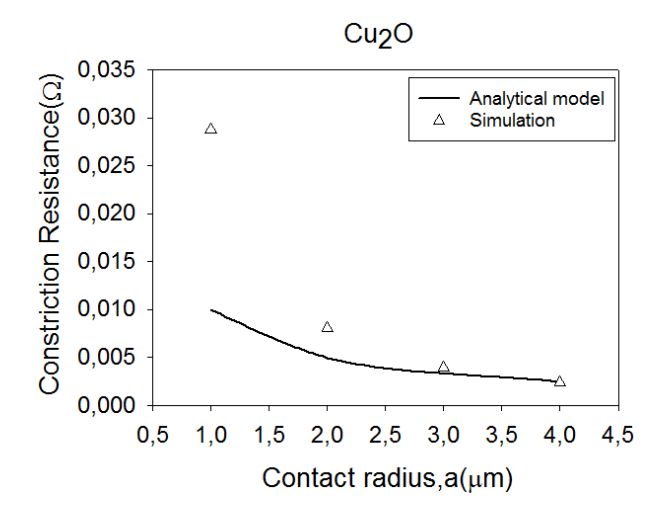


Fig.9. Contact temperature vs current for different a-spot radius. (Cu<sub>2</sub>O)

The simulation was conducted with a consistent nano-spot radius of 1  $\mu$ m, while varying the thickness of the oxide film from 1  $\mu$ m to 8  $\mu$ m. In the modeling process, we chose 1  $\mu$ m due to meshing challenges encountered with a thickness of 1  $\mu$ m.

It is deduced that, when considering a single conductive a-spot on the asperity surface, the analytical model precisely predicts the results obtained through finite element modeling (FEM), as shown in Figure 10.



**Fig.10.** Results of constriction resistance as a function of a-spot radius (F=1mN, I=1A, Oxide thickness=1 μm). (Cu<sub>2</sub>O)

Simulation results in the figure show that the temperature is inversely proportional to the contact radius (Fig.11).

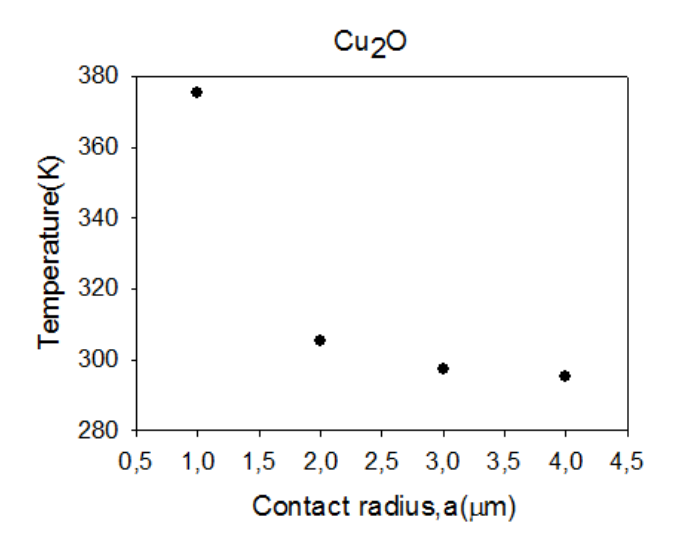


**Fig.11.** Results of contact temperature as a function of a-spot radius (F=1mN, I=1A, Oxide thickness=1 μm). (Cu<sub>2</sub>O)

The results for various oxide film thicknesses are illustrated in Fig. 12. It is apparent from the data that the thickness of the oxide film indeed exerts a notable influence compared to the aspot radius, leading to an increase in total resistance as the film thickness escalates from 1  $\mu$ m to 8  $\mu$ m. Moreover, the discrepancy between the analytical calculation and the Finite Element Model (FEM) exhibits a slight increase with a thicker oxide film.

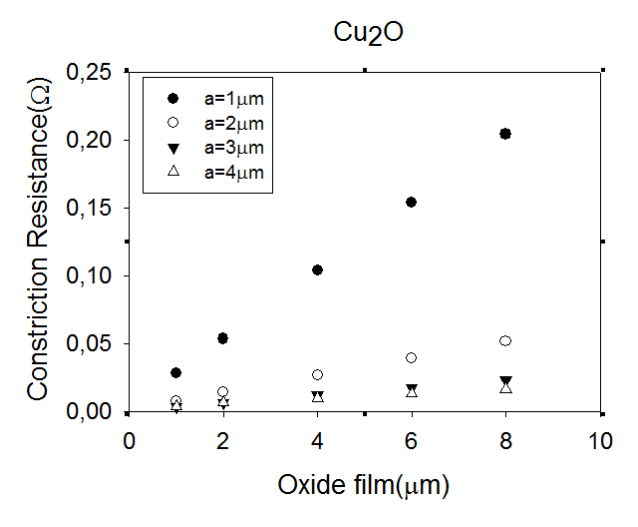


**Fig.12**. Results of constriction resistance as a function of a-spot radius (F=1mN, I=1A) (Cu<sub>2</sub>O)

The results presented in Figure 13 indicate that, similar to constriction resistance, the impact of the oxide film is more pronounced for the smallest contact radius, particularly highlighting the differences between the radius a=1 µm and the others.

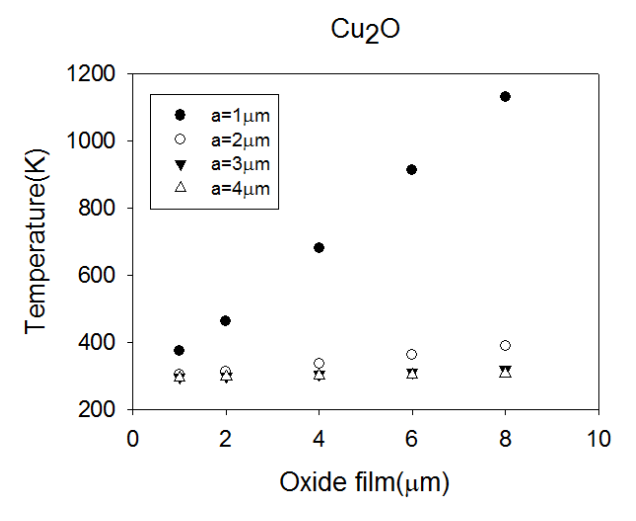
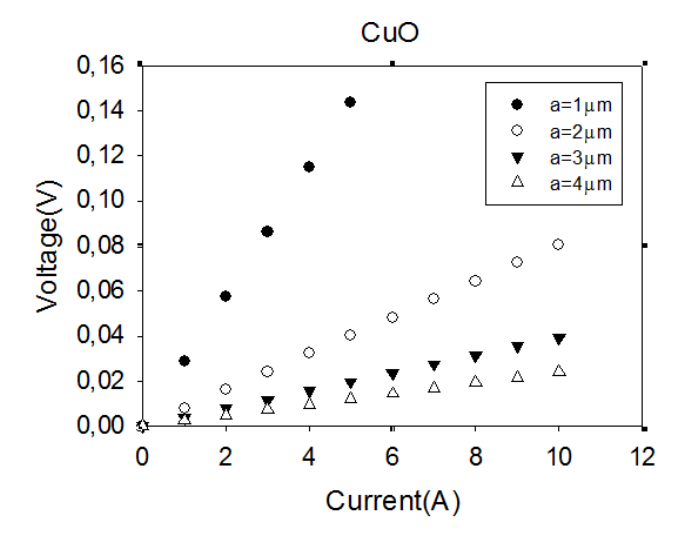


Fig.13. Results of contact temperature as a function of a-spot radius (F=1mN, I=1A). (Cu<sub>2</sub>O)

As the current is increased, resistive heating in the constriction a-spot leads to a rise in

temperature. Figures 14 and 15 depict the contact voltage drop over the contact and the temperature development up to the point of melting.



**Fig.14.** Contact voltage vs current for different a-spot radius (F=1mN, I=1A, Oxide thickness=1 μm). CuO

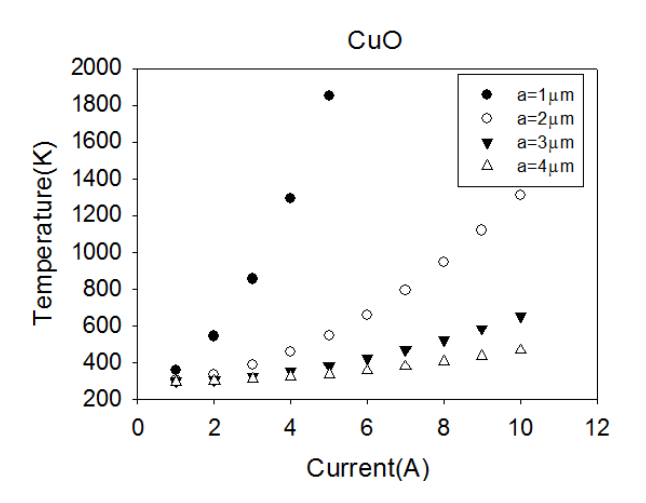


**Fig.15.** Contact temperature vs current for different a-spot radius (F=1mN, I=1A, Oxide thickness=1 μm). (CuO)

CuO exhibits similar trends as Cu<sub>2</sub>O in terms of contact voltage, constriction resistance, and temperature. However, the overall resistance of CuO-based contacts is higher than that of Cu<sub>2</sub>O-based contacts for identical contact areas. This observation suggests that CuO may have a more pronounced effect on constriction resistance and contact behavior, as illustrated in Figures 16, 17, and 18.

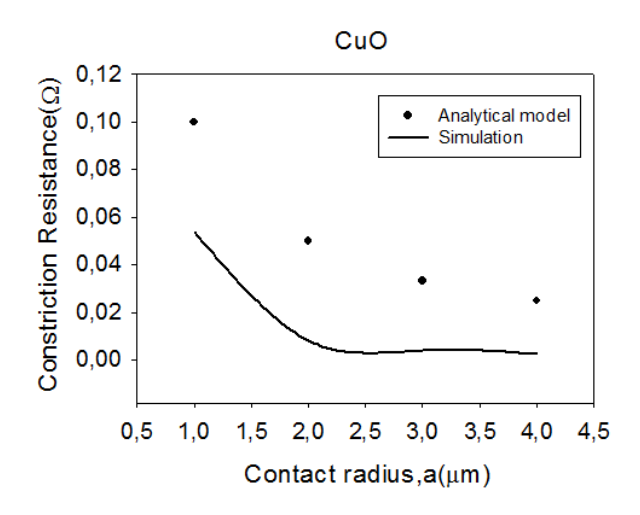


**Fig.16.** Relationship between constriction resistances by FEM results vs. a-spot radius of the electrode. (CuO)

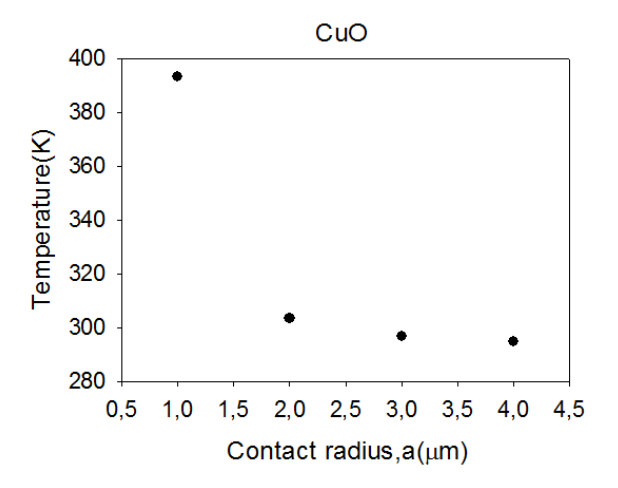


**Fig.17.** Relationship between contact temperature vs. a-spot radius of the electrode. (F=1mN, I=1A, Oxide thickness=1μm) (CuO)

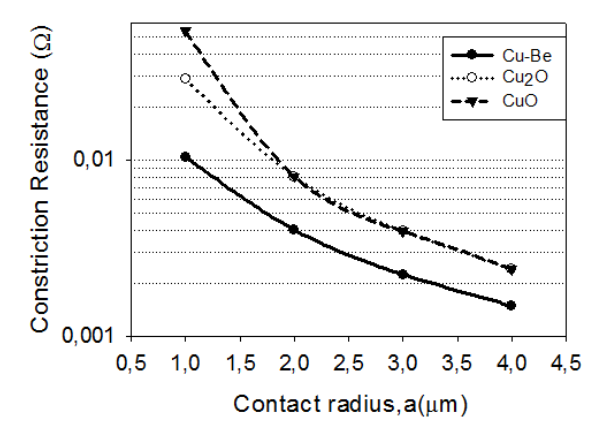


**Fig.18.** Contact resistance of Cu-Be without oxide and Cu-Be with CuO and Cu<sub>2</sub>O oxide versus the contact radius.

Constriction resistance increases with the ratio of oxide thickness (ct) to contact area in CuO-based contacts (Fig.19).

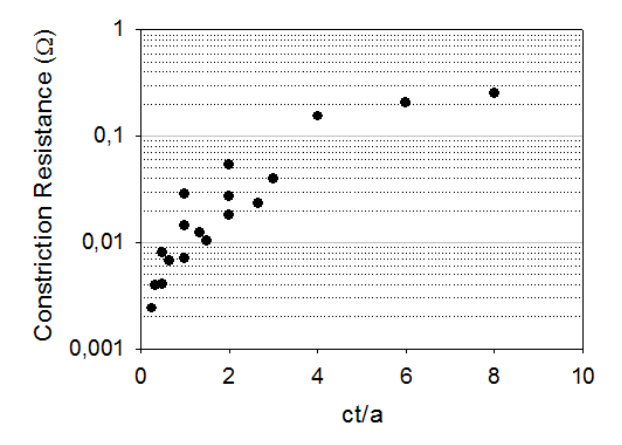


**Fig.19.** Constriction resistance vs ct/a F=1mN, I=1A, Oxide thickness=1 μm

## 4. CONCLUSIONS

We developed a method to assess how the contact structure influences constriction resistance using a physically simulated sample created through nanofabrication. Physical simulated samples with various diameters of the contact area were processed, and the resistances of the samples were repeatedly measured while changing the thickness of the upper electrode. After removing the influence of the electrode thickness, the resistance was found to be inversely proportional to the diameter of the contact area, aligning closely with an expression for constriction resistance.

Our demonstration illustrates that constriction resistance can be extracted from the measured resistance of the physically simulated sample. Physical simulation emerges as a robust tool, providing insights into the relationship between the contact structure and its contact resistance.

## 5. REFERENCES

- [1] Kogut, L., Electrical performance of contaminated rough surfaces in contact. Journal of Applied Physics, **2005**, 97(10), 103723.
- [2] Nabeta, Y., Saitoh, Y., Sawada, S., Iida, K., Hattori, Y, and Tamai, T., "Growth of oxide film on the tin-plated surface of connector contacts and its effect contact resistance characteristic," IEICE Technical Report, EMD2009-100, **2009**, pp. 133-136.

- [3] El Abdi, R., Benjemaa, N., Study of contact resistance for high copper alloys under indentation and insertion forces, International Journal of Systems Applications, Engineering & Development, 2008, 2(2)
- [4] Liu, H., Leray, D., Colin, S., Pons, P., Finite element modeling of nickel oxide film for Au-Ni contact of MEMS switches.61st IEEE Holm Conference on Electrical Contacts, Oct 2015, San Diego, United States.
- [5] Holm, R., Electric Contacts, Stockholm: Almqvist & Wiksells Akademiska Handböcker, **1946**, pp. 7-23.
- [6] Read; M. B., Lang, J. H., Slocum; A. H., Martens, R., "Contact Resistance in Flat-on-Flat and Sphere-on-Flat Thin Films, Proceedings of the 56 IEEE Holm Conference on Electrical Contacts, 2010, pp.348-355.
- [7] Holm, R., Electrical Contacts Theory and Applications, 4th Ed., Springer-Verlag, Berlin 1967
- [8] Zhong, L., Fan, X., Han, K., Chen, W., Qian, P., A degradation model for separable electrical contacts based on the failure caused by surface oxide film, Microelectronics Reliability, **2022**; 139, 114832
- [9] Wang, J-P., Cho, W. D., Oxidation Behavior of Pure Copper in Oxygen and/or Water Vapor at Intermediate Temperature, ISIJ International, Vol. 49, 2009, No. 12, pp. 1926– 1931.
- [10] Greenwood, J. A., "Constriction resistance and real area of contact," Brit. J. Appl. Phys., vol. 17, **1966**, pp. 1621-1632.
- [11] Slade, P.G., Electrical Contacts Principles and Applications, Marcel Dekker, New York 1999
- [12] Braunovic, M., Konchits, V., Myshkin, N., Electrical Contacts Fundamentals, Application and Technology, CRC Press Taylor Francis Group, **2007**
- [13] COMSOL Multiphysics 5.5: User's Guide
- [14] Wei Cheng, S., Chen, B.-S., Jian, S.-R., Hu, Y.-M., Le, P. H., Tuyen, L. T. C., Lee, J.-W. and Juang, J.-Y., Finite Element Analysis of Nanoindentation Responses in Bi2Se3 Thin Films, Coatings, **2022**, 12(10), 1554

- [15] Lindholm, P., Svahn, F., "Study of thickness dependence of sputtered carbon coating for low friction valve lifters", Wear, **2006**, 261 (3-4), pp. 241-250,
- [16] Korzhavyi, P. A., Johansson, B., Literature review on the properties of cuprous oxide Cu<sub>2</sub>O and the process of copper oxidation, Technical Report, TR-11-08, October 2011.